J Mater Sci (2008) 43:1776–1782
DOI 10.1007/s10853-007-2404-1

Comparative investigation on nanocrystal structure, optical, and electrical properties of ZnO and Sr-doped ZnO thin films using chemical bath deposition method

T. A. Vijayan · R. Chandramohan · S. Valanarasu · J. Thirumalai · S. P. Subramanian

Received: 28 October 2007 / Accepted: 13 December 2007 / Published online: 18 January 2008

Abstract This paper reports on the comparative investigation of structural and optical properties of nano thin films of ZnO and Sr-doped ZnO (SZO) onto glass substrates synthesized by a two-step chemical bath deposition (CBD) technique. The mode of crystallization, structural properties, and morphologies have been investigated. The films are polycrystalline in nature with hexagonal phase having (002) preferential orientation. The typical crystallite size is also estimated and found to be around 30–80 nm. The shifts in optical band gap of the SZO films are estimated to be ~3.25–3.27 eV with respect to the ZnO film and the refractive index is 2.35. The room temperature resistivity is of the order of ~2,000 Ωcm. Thermoemf measurements show that films are of *n*-type. The sensitivity of the films was studied as a function of their temperature 275–575 K for a fixed ethanol concentration (400 ppm). The films have been tested for cross sensitivity for different gases and it has been confirmed that these are highly sensitive and selective for ethanol vapors around 200 °C in air atmosphere.

T. A. Vijayan · R. Chandramohan (✉) · J. Thirumalai
Department of Physics, Sree Sevugan Annamalai College, Devakottai 630303, India
e-mail: chandru17@yahoo.com

S. Valanarasu
Department of Physics, Ananda College, Devakottai 630303, India

S. P. Subramanian
Department of Chemistry, Sree Sevugan Annamalai College, Devakottai 630303, India

Introduction

Zinc oxide (ZnO) is a versatile material of compound semiconductors with excellent properties and has extensive applications in electronics, photoelectronics, sensors, and catalyst. ZnO thin films have attracted considerable attention because they can be tailored to possess high electrical conductivity, high infrared reflectance, and high visible transmittance by different coating techniques. The remarkable properties of ZnO are due to its wide direct band gap of 3.37 eV [1, 2]. Sr-doped ZnO (SZO) film is one of the promising alternatives to indium tin oxide (ITO) thin films. This is because, zinc is a cheap and abundant raw material, and has comparable electrical and optical properties [3, 4]. SZO coatings exhibit high transparency and low resistivity and these materials are suitable for fabricating transparent electrodes in solar cells, gas sensors, MEMS, love wave filter applications, and ultrasonic oscillators [5]. Optical and electrical properties of SZO thin films could be modified by thermal treatment in a reducing atmosphere [6]. The chemical bath deposition (CBD) technique is an open-bath wet-chemical method that has been extensively employed for the synthesis of metal oxide thin films [7, 8]. The aim of this work is to investigate the influence of the preparation conditions on structural, optical, and electrical properties of ZnO and SZO films prepared using CBD method. The films were prepared from colloidal suspensions containing different Sr concentrations and deposited using dip-coating technique. The structural characteristics were studied by X-ray diffraction (XRD), the morphological features and percentage of concentrations were studied by scanning electron microscope (SEM) and energy dispersive X-ray analysis (EDX). Thickness of the film was measured using Dektak measurements. The electrical and optical properties were

investigated by resistivity measurement, photoluminescence (PL) and UV-visible spectrophotometer (UV-Vis), respectively. A gas sensor was fabricated using the principle of resistivity measurement and its sensitivity at various temperatures were estimated.

Experimental procedure

Synthesis

ZnO thin films were grown using a two-step CBD technique using a solution comprising 0.1 M zinc sulphate, 0.2 M sodium hydroxide with a pH value of 9 ± 0.2 deposited at room temperature followed by a dip in water bath of temperature around 90 °C under optimized condition. For Sr-doped ZnO (SZO) thin films $Sr_2(SO4)_3$ was used at a concentration of 0.1 mM (Sample B) and 1 mM (Sample C). Before deposition, the glass substrates were cleaned by chromic acid followed by cleaning with acetone. The well-cleaned substrates were immersed in the chemical bath for a known standardized time followed by immersion in hot water for the same time for hydrogenation. The process of solution dip (step 1) followed by hot water dipping (step 2) is repeated for known number of times. The cleaned substrate was alternatively dipped for a predetermined period in sodium zincate bath and water bath kept at room temperature and near boiling point, respectively. According to the following equation, the complex layer deposited on the substrate during the dipping in sodium zincate bath will be decomposed to ZnO due to dipping in hot water.

$$ZnSO_4 + 2NaOH \rightarrow Na_2ZnO_2 + H_2SO_4 \uparrow$$

$$Na_2ZnO_2 + H_2O \rightarrow ZnO + 2NaOH$$

Part of the ZnO so formed was deposited onto the glass substrate as a strongly adherent film and the residue formed as a precipitate.

Characterization studies

The crystalline structure was determined by X-ray diffraction using X'pert PRO (PANalytical) diffractometer with Cu Kα radiation ($\lambda = 0.15405$ nm) and employing a scanning rate of 5° min^{-1}. The particle size and morphology was examined in a scanning electron microscope (SEM) Hitachi S-3000H model. For SEM studies the samples are pre-coated with Au sputtering using fine coat ion sputter JFC-1100 model instrument. Photoluminescence (PL) spectra were recorded with a VARIAN Cary Eclipse spectrophotometer equipped with a 150 W xenon lamp as the excitation source. Optical transmittance was measured by Perkin Elmer Lambda 35 UV-Vis spectrophotometer. All the measurements were performed at room temperature.

Results and discussion

The crystallographic structure of the films has been studied by XRD. Figure 1a shows the XRD spectrum of ZnO and SZO films deposited on the glass substrate under optimized condition. It can be seen from the XRD data, that all samples are polycrystalline in nature and exhibit single-phase ZnO hexagonal wurtzite structure [9] ($P6_3mc$ space group, JCPDS, 36-1451). All peaks in recorded range were identified. The XRD pattern clearly showed the polycrystalline nature of the ZnO and SZO films, whose *c*-axis was preferentially oriented normal to the glass substrate [9]. In other words, grains of undoped and doped films are mainly grown with *c*-axis vertical to the glass substrate. Hence, the multiple coating or the piling up of each ZnO and SZO film was considered not to disturb the overall growth of the films with *c*-axis orientation. The *c*-axis orientation was also reported for ZnO films deposited on oxide glass substrates by CVD [10], spray pyrolysis [11], sol-gel process [12], and DC magnetron sputtering [13]. Therefore, the *c*-axis orientation may be a common phenomenon in the ZnO film deposition by the chemical process using organozinc compounds. Such preferred basal orientation is typically observed in SZO films [5, 14, 15]. Moreover, from the recorded spectrums (Fig. 1a and b), the minor diffraction peaks of (102) and (103) are also visible and is in consistent with those reported for ZnO films [16].

From Fig. 1b, it is evident that, a very small shift of the diffraction lines is expected more for the doped materials. However, this shift can be measured more obvious in the nanocrystalline sample C, because the strontium concentration is high and the width of the diffraction lines is broadened due to the small size of the crystallites. The crystallite sizes of these nanoparticles were calculated using the Debye Scherrer's equation and the estimated average crystallite size ranges from 30 to 80 nm (Table 1). The lattice constants calculated from the most prominent peaks and the ratio of relative intensities $I(002)/I(101)$ in the diffraction pattern of ZnO and SZO films at room temperature, respectively, are given in Table 1. The lattice constants calculated are found to be in good agreement with ASTM and standard JCPDS data for ZnO powder. The texture coefficient is calculated to describe the preferential orientation using the expression [17]:

$$\mathrm{TC}(hkl) = \frac{I(hkl)/I_0(hkl)}{N_r^{-1}\sum_{N_r} I(hkl)/I_0(hkl)} \quad (1)$$

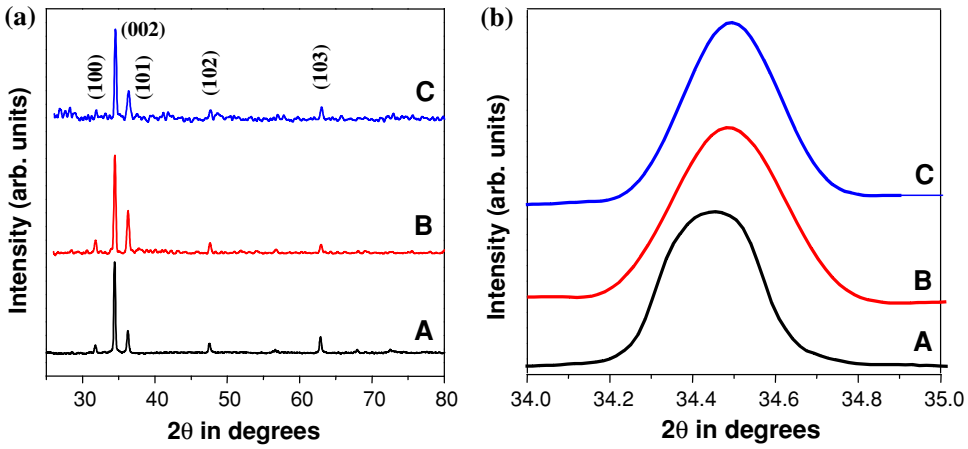

Fig. 1 (**a**) X-ray diffraction patterns of the ZnO and SZO thin films. (A) Pure ZnO, (B) SZO (100:1), (C) SZO (10:1) having film thickness: 1.6 μm. (**b**) Enlarged region of the (002) plane to indicate the shift in XRD peak due to Sr-doping concentration

where I is the measured intensity and I_0 is the measured standard intensity. The texture coefficient is calculated for the crystal planes (002) and (101). The value of the texture coefficient indicates the maximum preferred orientation of the films along the diffraction plane, meaning that the increase in preferred orientation is associated with increase in the number of grains along that plane. As can be seen from the Fig. 1a, the samples correspond to B and C indicates that the diffraction angles of all of SZO thin films are departed from 34.45° slightly, which may be due to the doping of strontium to zinc leading to the aberrance of ZnO crystal lattice. The preferential orientation of the SZO films is found to be along (002) direction and the peak is very sharp. Other reflections appear relatively weak.

Morphology

Figure 2a–c shows the scanning electron micrograph (SEM) of ZnO and SZO films deposited at room temperature. The SEM micrographs show the uniform polycrystalline surface of the film with a hexagonal morphology consistent with $P6_3mc$ crystal structure with an average particle size of 500 nm. From Fig. 2b and c it can be seen that, films grown at room temperature by varying Sr concentration, the slightly agglomerated particles are seen and less voids are present in the film. The concentration of voids of a purely stoichiometric film will decrease usually with doping if doped externally. But in our samples, the increase in grain size and the adjustment of stoichiometry during film formation in a competitive and entirely new environment produces different morphologies. For small percentage of dopant concentration, the micrograph shows no significant change in morphology. From EDAX, the quantitative analyses were carried out for Zn, O, and Sr at various points on the sample. The average of the atomic percentage of Zn:O:Sr was 72:26:2. Along with Zn element, some Si content is also revealed in EDX that is originating from the glass substrates.

Optical properties of undoped and Sr-doped ZnO thin films

Figure 3a and b shows the photoluminescence spectrum of the ZnO and SZO thin films grown on glass substrate. ZnO is a nonstoichiometric oxide and is known to contain zinc-ion excess defects based on the presence of either zinc interstitial or oxygen vacancies. It is well known for photoluminescence of ZnO that visible emissions at various energies are caused by lattice defects of vacancies, charged interstitial, and antisites [18, 19]. All these defects will have their energy levels in the forbidden gap. The visible photoluminescence observed in this study indicates that the ZnO and SZO nano thin films have different kinds of lattice defects. Undoped and doped films show two photoluminescence emission

Table 1 Lattice constants and $I(002)/I(101)$ ratios of ZnO and SZO films deposited at the room temperature

Sample details	Crystallite size (nm)	Lattice constants		Relative intensity $I(002)/I(101)$
		a_0 (nm)	c_0 (nm)	
JCPDS (36-1451)	–	0.3244	0.5205	0.560
A	82	0.3246	0.5208	0.780
B	28.5	0.3248	0.5194	1.806
C	27	0.3255	0.5200	1.938

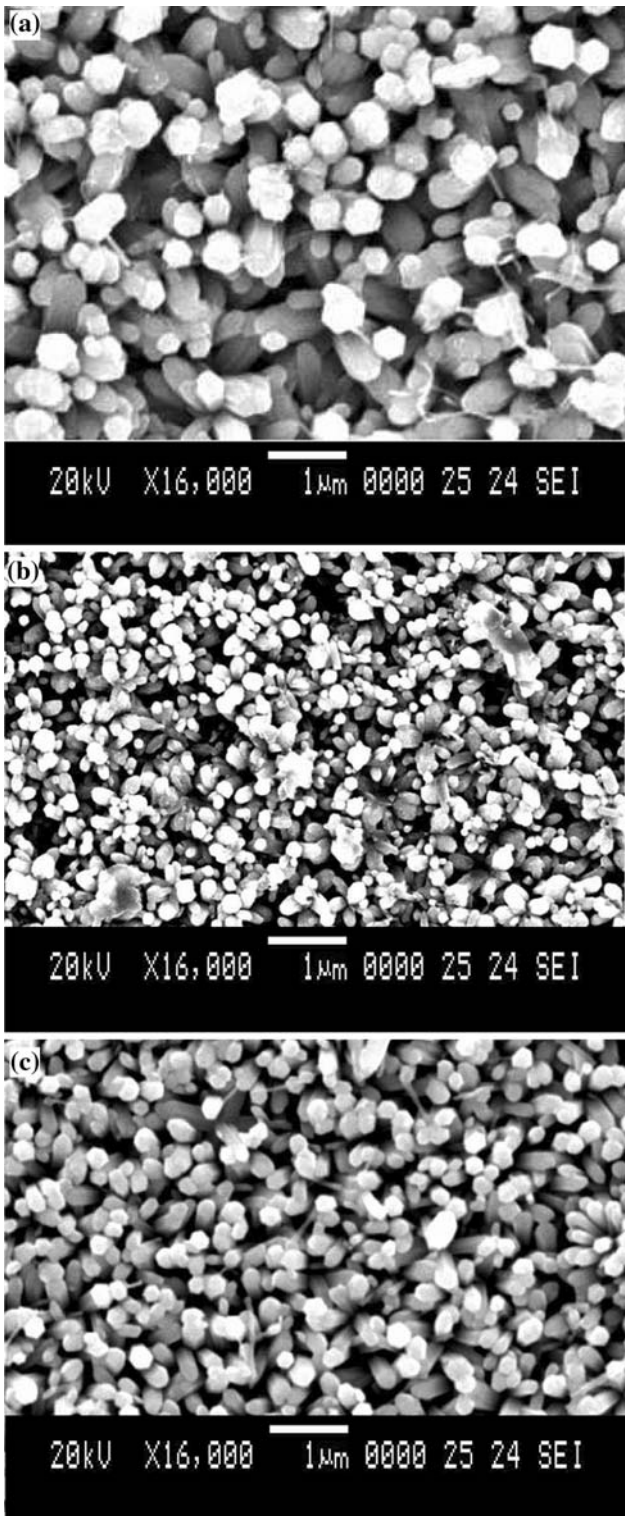

Fig. 2 SEM images of undoped and Sr-doped ZnO thin films with different strontium contents. (**a**) ZnO, (**b**) ZnO:Sr (0.1 mM), and (**c**) ZnO:Sr (1 mM)

peaks for all the thin films. The Fig. 3b of the ZnO and SZO samples was localized at around 3.25 eV, which correspond to the band-to-band transition. While, Fig. 3a corresponds to the sub-band transition located at about 2.55 eV, which would be roughly nearer to the reported value [20]. The deep level emission corresponds to the zinc vacancy (V_{zn}) and anti site defect (O_{zn}) as suggested by Wang et al. [20]. It has been proposed that the blue green emission in the material might be associated to a transition with a self activated center formed by a doubly ionized zinc vacancy Vzn^{2-} and the single-ionized interstitial Zn^{+} at the one end/or two nearest neighbor interstitial sites [21, 22]. The PL spectra reveal that, the intensity of the band edge emission peak decreases, with the increase in intensity of the deep level emission peak, in the undoped and doped films coated on glass substrate. Doping is an effective approach to adjust the Fermi energy level for semiconductors. The relationship between electron concentration and the Fermi level can be written as [23]

$$\eta_e = 2\left(2\pi m^* kT/h^2\right)^{3/2} \exp\left[(E_F - E_C)/kT\right] \quad (2)$$

where η_e is the electron concentration, m^* is the electron effective mass, k is Boltzmann's constant, h is Planck's constant, T is the absolute temperature, and E_F and E_C are energies at the Fermi level and the bottom of conduction band, respectively.

Figure 4 shows the optical transmission spectra of ZnO and SZO films in the visible range prepared at room temperature under optimized condition. It can be seen from Fig. 4a (samples B and C), when the concentration of doping is increased, the transmittance of the SZO film increases gradually. The transmittance of the SZO film corresponding to samples B and C from Fig. 4a which is higher than 75% for wavelengths over 400 nm.

Figure 4b shows the optical band gap of the ZnO and SZO thin films estimated by extrapolation of the linear portion of α^2 versus $h\nu$ plots using the relation $\alpha h\nu = A(h\nu - E_g)^{n/2}$, where α is the absorption coefficient, $h\nu$ the photon energy, and E_g is the optical band gap. For different n values, a good linearity was observed at $n = 1$ (direct allowed transition) which is found to be the best fit for these films. The optical band gap of the SZO thin film has increased from 3.25 to 3.27 eV with respect to the band gap of intrinsic ZnO (3.2 eV) [24]. Assuming doping levels well below Mott's critical density, the change in optical band gap can be explained in terms of Burstein–Moss band gap widening and band gap narrowing due to the electron–electron and electron–impurity scattering [25–27]. At high doping concentrations, Fermi level lifts into the conduction band. Due to filling of the conduction band, absorption transitions occurs between valance band and Fermi level in the conduction band instead of valance band and bottom of the conduction band. This change in the absorption energy levels shifts the absorption edge to higher energies (blue shift) and leads to the energy band broadening (ΔE_g), which can be calculated by the following equation [28]:

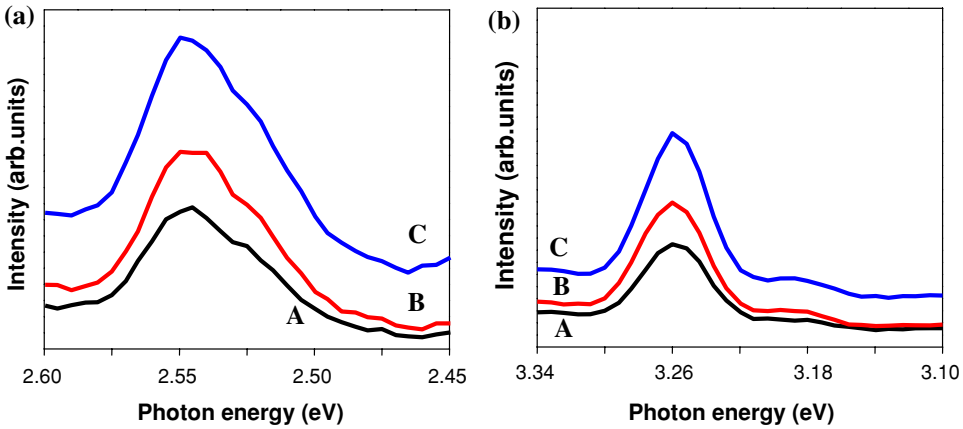

Fig. 3 The PL spectra of ZnO and SZO thin films recorded at room temperature

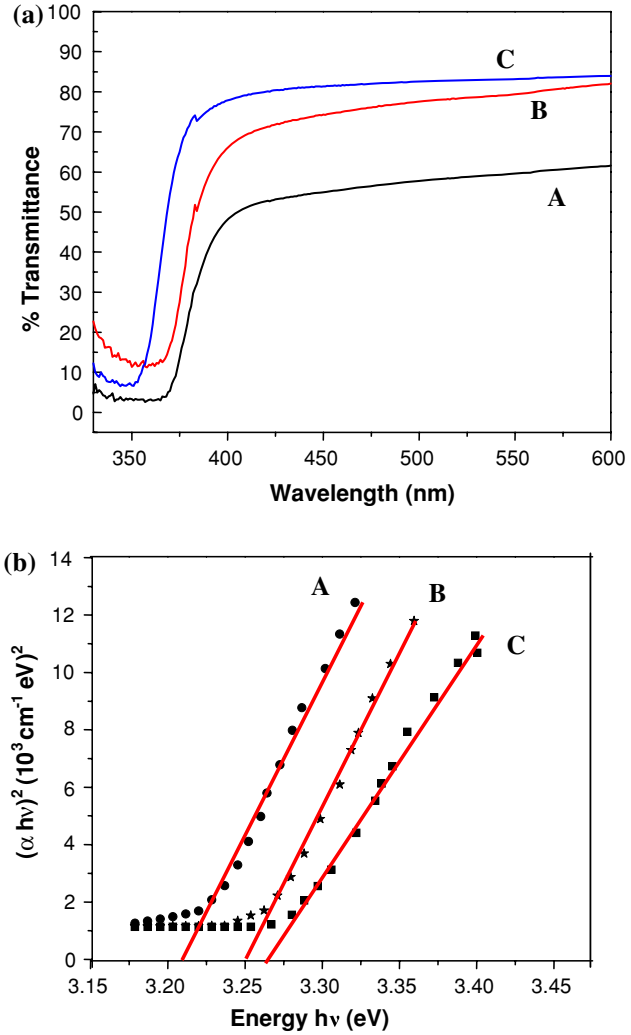

Fig. 4 (**a**) The optical transmittance of the undoped and Sr-doped ZnO thin films coated on glass substrate having film thickness 1.6 μm. (**b**). Plot of $h\nu$ versus $(\alpha h\nu)^2$ for undoped and Sr-doped ZnO thin film coated on glass substrate

$$\triangle E_g = \frac{h_2}{8m^*}\left(\frac{3}{\pi}\right)^{2/3}\eta_e^{2/3} \tag{3}$$

where h is the Planck's constant, m^* the electron effective mass in conduction band, and η_e is the carrier concentration. While on Sr-doping into the ZnO matrix can explain the increase in shift in the band gap value indicating that either it may be due to any charged defects or the charged defects formed had been neutralized by other defects. Hence, the blue shift in the band gap value during Sr-doping suggest an increase in the n-type carrier concentration, most of the Sr ions must be incorporated as interstitial donors into the structure rather than substitutional acceptors. As a result, the carrier concentration (η_e, in cm^{-3}) was estimated using Eq. 3 for samples A, B and C are 10.015×10^{21}, 27.12×10^{21} and 153.98×10^{21}, respectively. In addition, the refractive index as a function of wavelength for ZnO and SZO thin films corresponding to the samples A, B and C was calculated using Eq. 4 [29] to be 2.34, 2.33 and 2.32, respectively, which is close to the value in the literature [4, 30, 31].

$$\frac{(n^2-1)}{(n^2+2)} = 1 - \sqrt{E_g/20} \tag{4}$$

where the symbols have the usual meaning.

Electrical properties

Besides the optical properties, the electrical properties are also an important aspect of the performance of the SZO thin films. Doping of ZnO with group II-A elements such as B, Sr, or In increase the n-type conductivity [32]. The electrical conductivity of ZnO is directly related to the number of electrons, electrons formed by the ionization of the interstitial zinc atom, and the oxygen vacancies [33]. It can be seen from Fig. 5a that, the electrical resistivity of

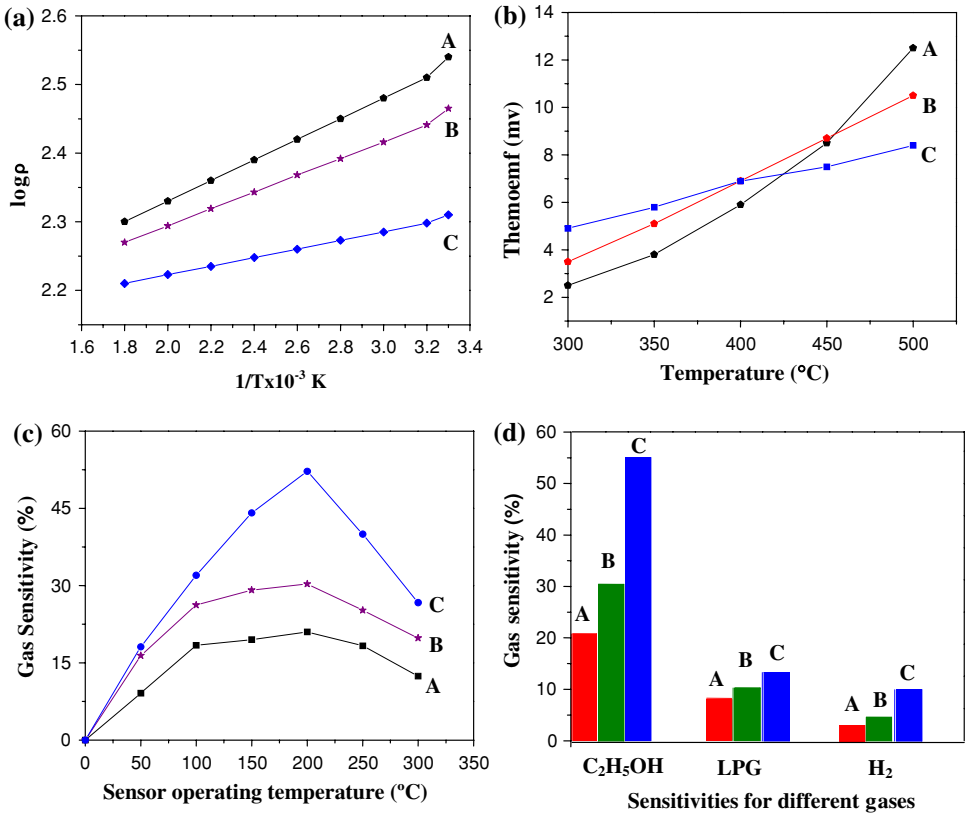

Fig. 5 Electrical and gas sensor studies for (A) ZnO, (B) SZO (0.1 mM), (C) SZO (1 mM) using four-probe method. **(a)** Plot of log(ρ) versus (1/T). **(b)** Variation of thermoemf with temperature. **(c)** Sensitivity versus operating temperature. **(d)** Sensitivities for different gases

the doped films is lower than that of the undoped films. The lowest d.c. electrical resistivity value of the SZO film (sample C) is ~2,000 Ωcm, measured as a function of temperature in the range 300–500 K using four-probe method. It is found that resistivity decreases linearly with increasing temperature especially in the sample C when compared to the other samples (B and C), exhibiting a semiconducting nature of the film.

The thermal activation energies (E_a) are calculated by the resistivity relation,

$$\rho = \rho_0 \exp(E_a/KT) \quad (5)$$

where ρ_0 is the pre-exponential factor, K is Boltzmann's constant and T is the absolute temperature. The values of the activation energies for the ZnO and SZO films corresponding to samples A, B, and C are estimated to be 6.6, 4.2, and 2.1 meV, respectively. Thermoemf developed across the sample was measured as a function of temperature in dark within the temperature range 300–500 K using four-probe method. Figure 5b shows the variation of thermoemf with temperature for the ZnO and SZO samples deposited at room temperature. The polarity of the thermally generated voltage at the hot end is positive with respect to cold end, confirming that the films are semiconducting n-type.

The four-probe fused conductivity measurement system gas sensor designed indigenously was used to determine the electrical conductivity of the films. Figure 5c shows the sensitivity as a function of sensor operating temperature for doped and undoped film for ethanol vapor in air atmosphere. It is evident from these results, that the sensitivity of the undoped ZnO film is very poor compared to that of SZO in different concentrations. The sample C containing 1 mM of SZO matrix manifests a maximum sensitivity of 55% to alcohol vapors at an operating temperature of 200 °C. Figure 5d shows the sensitivity of the elements in different gas atmospheres. It is seen that in all the cases, the ethanol gas sensitivity is exceptionally high, while the sensitivity to liquefied petroleum gas (LPG) and hydrogen (H_2) remains very poor. To increase the basic sites, which catalyses the oxidation of C_2H_5OH, it is essential to dope ZnO with element like Sr. It may be concluded that, the SZO film (Sample C) is effective to improve the sensitivity and also retains the selectivity to ethanol vapor with a maximum sensitivity of 55%, which is suitable for commercial use. SZO seems to be one of the most promising semiconducting materials for the detection of ethanol vapor.

Conclusion

Polycrystalline, hexagonal ZnO and SZO nano thin films with (002) preferential orientation have been deposited from aqueous solutions using a modified two-step CBD technique onto a glass substrate. Optical absorption

indicated the shift in band gap to be around 3.24–3.27 eV with respect to band gap of ZnO matrix and refractive index to be around 2.34–2.29. The transmittance became higher for SZO films with increase in doping concentration. In the Sr doped ZnO films, the films were oriented more preferentially along the (002) direction, as the grain size of the films increased, the transmittance also became higher and the electrical resistivities decreased. Films doped with 1 mM Sr had stronger orientation along the (002) direction, larger the grain size, higher the conductivity, and transmittance than that of the other metal doped films. It is shown that doped ZnO thin films deposited with a CBD technique can have high sensitivity to ethanol vapor with a maximum of 55%. Finally, a better sensitivity can be observed for SZO films, and especially for higher concentration.

Acknowledgement The authors T.A. Vijayan and R. Chandramohan thank University Grants Commission, New Delhi, India for the financial support.

References

1. Ryu YR, Zhu S, Budai JD, Chandrasekhar HR, Miceli PF, White HW (2000) J Appl Phys 88:201
2. Wang L, Giles NC (2003) J Appl Phys 94:973
3. Minami T, Suzuki S, Miyata T (2001) Thin Solid Films 53:398
4. Chu S-Y, Water W, Liaw J-T (2003) Ultrasonics 41:133
5. Chu S-Y, Chen T-Y, Water W (2005) IEEE Trans Ultrason Ferroelectr Freq Control 52:2308
6. Water W, Yan Y-S (2007) Thin Solid Films 515:6992
7. Boyle DS, Govender K, O'Brien P (2003) Thin Solid Films 483:431
8. Peiró AM, Domingo C, Peral J, Domenech X, Vigil E, Hernández-Fenollosa MA, Mollar M, Marí B, Ayllón JA (2005) Thin Solid Films 483:79
9. Powder diffraction files, Joint Committee on Powder Diffraction Standards, ASTM, Philadelphia, PA, 1967 Card 36-1451
10. Cheng H-C, Chen C-Fu, Lee C-C (2006) Thin Solid Films 498:142
11. Aranovich J, Ortiz A, Bube RH (1979) J Vac Sci Technol 16:994
12. Tang W, Cameron DC (1994) Thin Solid Films 238:83
13. Hata T, Minamikawa T, Morimoto O, Hada T (1979) J Cryst Growth 47:171
14. Aktaruzzaman AF, Sharma GL, Malhotra LK (1991) Thin Solid Films 198:67
15. Hu J, Gordon RG (1992) J Appl Phys 71:880
16. Izaki M (1999) J Electrochem Soc 146:4517
17. Barret C, Massalki TB (1980) Structure of metals. Pergamon, Oxford, pp 204
18. Shi CS, Fu ZX, Guo CX, Ye XL, Wei YG, Deng J, Shi JY, Zhang GB (1999) J Electron Spectrosc Relat Phenom 103:629
19. Kohan AF, Ceder G, Morgan D, Van de Walle CG (2000) Phys Rev B 61:15019
20. Wang J, Du G, Zhang Y, Zhao B, Yang X, Liu D (2004) J Cryst Growth 263:269
21. Studenikin SA, Golego N, Cocivera M (1998) J Appl Phys 84:4
22. Minami T, Nanto H, Takata S (1981) J Lumin 63:2425
23. Sze SM (1981) Physics of semiconductor devices, p 84
24. Pankove JI (1975) Optical progress in semiconductors. Dover Publications, New York
25. Burstain E (1954) Phys Rev 93:638
26. Moss TS (1954) Proc Phys Soc London Ser B 67:775
27. Sernelius SE, Berggren KF, Jin ZC, Hamberg I, Granavist CG (1988) Phys Rev B 37:10244
28. Lee HW, Lau SP, Wang YG, Tse KY, Hng HH, Tay BK (2004) J Cryst Growth 268:596
29. Dimitrov V, Sakka S (1996) J Appl Phys 79:1736
30. Lide DR (2005) CRC handbook of chemistry and physics, vol 10, CRC press, p 230
31. Cetinorgu E, Goldsmith S, Boxman RL (2007) Surf Coat Technol 201:7266
32. Jung SJ, Han YH, Koo BM, Lee JJ, Joo JH (2005) Thin Solid Films 475:275
33. Sukkar MH, Tuller HL (1984) Adv Ceram 7:71